Characterizing a turbidite system in Canterbury Basin, New Zealand, using seismic attributes and distance-preserving self-organizing maps

Tao Zhao[1], Jing Zhang[1], Fangyu Li[1], and Kurt J. Marfurt[1]

Abstract

Recent developments in seismic attributes and seismic facies classification techniques have greatly enhanced the capability of interpreters to delineate and characterize features that are not prominent in conventional 3D seismic amplitude volumes. The use of appropriate seismic attributes that quantify the characteristics of different geologic facies can accelerate and partially automate the interpretation process. Self-organizing maps (SOMs) are a popular seismic facies classification tool that extract similar patterns embedded with multiple seismic attribute volumes. By preserving the distance in the input data space into the SOM latent space, the internal relation among data vectors on an SOM facies map is better presented, resulting in a more reliable classification. We have determined the effectiveness of the modified algorithm by applying it to a turbidite system in Canterbury Basin, offshore New Zealand. By incorporating seismic attributes and distance-preserving SOM classification, we were able to observe architectural elements that are overlooked when using a conventional seismic amplitude volume for interpretation.

Introduction

During the past two decades, seismic attributes have improved substantially not only in innovative algorithm development but also in their use in integrated interpretation. In addition to highlighting features of geologic interest, multiple attributes can be combined for seismic facies classification. Three-dimensional corendering of multiple attributes is an effective way to visualize subtle features that may be overlooked on conventional amplitude data. Unfortunately, a 32-bit color model (red-green-blue [RGB], hue-lightness-saturation [HLS], or cyan-magenta-yellow [CMY] color gamut modulated by alpha blending) limits us to combining at most four attributes. Furthermore, although some attribute combinations form natural pairs or triplets, such as dip magnitude, dip azimuth, and coherence (Marfurt, 2015), others do not, resulting in corendered images that are difficult to interpret. Seismic facies classification algorithms attempt to mimic human pattern recognition and can be applied to a more arbitrary collection and greater number of attributes. Feeding multiple attributes into a classification algorithm enables interpreters to analyze different aspects of seismic response (energy, frequency, phase, geometry, texture, etc.) simultaneously, generating a map of facies or correlating seismic responses to engineering/production data (Roy et al., 2013; Zhang et al., 2015).

The rapid invention of fresh seismic attributes has greatly expanded the interpreter's arsenal for seismic interpretation. However, such great numbers of attributes put a serious challenge on inexperienced seismic interpreters: Which attributes are most suitable to use? In general, we prefer mathematically well designed, independent attributes with intuitive geologic and geophysical meaning (Barnes, 2007). In addition, attribute selection is highly target oriented, which means we may use formation attributes to map lithology change, structure attributes for deformation, and edge-detection attributes for fractures. In contrast, it may be inappropriate to use spectral magnitude to map a fault. Modern seismic interpretation often involves facies classification in which attributes serve as the input. The results of such applications are highly sensitive to the attribute selection process. During our analysis, we chose several attributes that, as human interpreters, we thought represented important architectural elements. The classification scheme saw things differently such that these attributes needed to be rejected. In this paper, we therefore not only present attributes that were used in seismic facies classification to characterize the turbidite systems but also discuss attributes that were eliminated during the classification.

Seismic attributes are routinely used by interpreters. In contrast, seismic facies classification, deeply rooted in statistics, and requiring significant computing power, is less commonly used. During the past 20 years, several alternative algorithms have been proposed and success-

[1]The University of Oklahoma, ConocoPhillips School of Geology and Geophysics, Norman, Oklahoma, USA. E-mail: tao-zhao@ou.edu; jing.zhang@ou.edu; fangyu.li@ou.edu; kmarfurt@ou.edu.

Manuscript received by the Editor 27 June 2015; revised manuscript received 10 October 2015; published online 15 February 2016. This paper appears in *Interpretation*, Vol. 4, No. 1 (February 2016); p. SB79–SB89, 13 FIGS., 1 TABLE.

http://dx.doi.org/10.1190/INT-2015-0094.1.

fully applied to computer-assisted seismic facies classification (Zhao et al., 2015). The Kohonen self-organizing map (SOM) (Kohonen, 1982) is one of the most widely accessible techniques in commercial software packages that produces reasonably high quality seismic facies maps. The SOM preserves the topological connections among clusters, which is a preferred attribute for visualization when using similar colors for similar facies (Strecker and Uden, 2002; Roy et al., 2013). However, traditional Kohonen SOM does not preserve the distance in input space, which may result in an over-/undershrinking of the clusters in the SOM latent space. A latent space is a lower dimensional space, into which the original input data are projected. Analyzing data in a particular latent space may discover data properties that are easily overlooked in the original space. A frequently used example would be projecting multiattribute data using principal component analysis (PCA) and crossplotting the first two principal components. Such a crossplot serves as a 2D latent space of the original multiattribute data. Intuitively, data vectors with similar seismic attribute responses should belong to similar facies. However, after mapping into a latent space in which the SOM nodes live, the projection of such data vectors may no longer maintain the same degree of similarity between each other. For this reason, we need to introduce some constraints to maintain the consistency of similarity among clusters in the n-dimensional input and (in our examples) 2D latent space.

During the development of SOM, several variants have been introduced to address this issue, such as grouping neuron SOM (Rubio and Gimnez, 2003), adaptive coordinate SOM (Merkl and Rauber, 1997), and double SOM (Wang et al., 2002), to name a few. These algorithms are all based on Himberg's contraction model (Himberg, 2000), which means that the adjustment of distance among SOM nodes in the SOM latent space is only contraction, not expansion. In this study, we implement Shao and Yang's (2012) distance-preserving SOM (DPSOM), in which the distance adjustment among SOM nodes can be both contraction and expansion.

We begin our paper by discussing the geologic setting in the Canterbury Basin, followed by the attribute expression of a turbidite system. Then, we introduce DPSOM, apply it to a simple synthetic, and compare it with traditional Kohonen SOM. Then, we apply DPSOM to a Canterbury Basin, New Zealand, turbidite with the goal of mapping key architectural elements. We conclude with a final comparison to traditional SOM, summarizing the value and limitations of SOM in general.

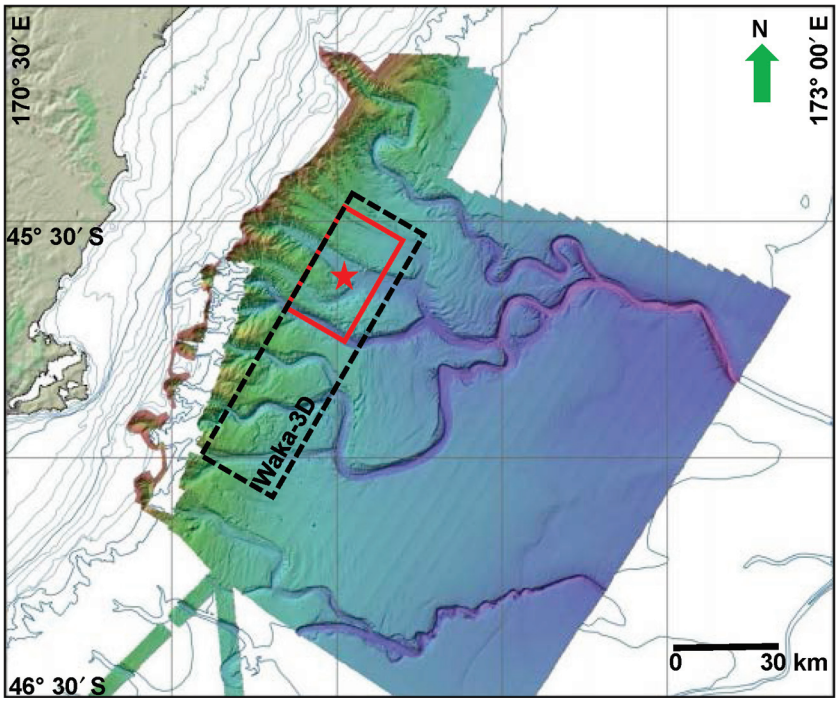

Figure 1. A map showing the location of the 3D seismic survey acquired over the Canterbury Basin, offshore New Zealand. The black rectangle denotes the limits of the Waka-3D survey, whereas the smaller red rectangle denotes the part of the survey shown in subsequent figures. The colors represent the relative depth of the current seafloor, warm being shallower and cold being deeper. Current seafloor canyons are delineated in this map, which are good analogs for the paleocanyons in Cretaceous and Tertiary turbidites (modified from Mitchell and Neil, 2012).

Geologic setting

We examine a turbidite system imaged in the Waka-3D seismic survey acquired over the Canterbury Basin, offshore New Zealand, which has been generously made public by New Zealand Petroleum and Minerals. Figure 1 shows the location of this survey, in which the red rectangle corresponds to the area shown in subsequent figures. The study area lies on the transition zone of continental slope and rise with an abundance of paleocanyons and turbidite deposits of Cretaceous and Tertiary ages. These sediments were deposited in a single, tectonically driven transgressive-regressive cycle (Uruski, 2010). Potential source rocks in the Canterbury Basin are Late Jurassic coaly sediments, Late Cretaceous coaly sediments, and Paleocene marine shales. Reservoir rocks are fluvial, estuarine, and marine sandstones of Cretaceous and Tertiary (Sutherland and Browne, 2003). Being a very recent and underexplored prospect, publicly available comprehensive studies of the Canterbury Basin are somewhat limited. The modern seafloor canyons shown in Figure 1 are good analogs of the deeper paleocanyons illuminated by the 3D seismic amplitude and attribute data.

In this study, our goal is to analyze a turbidite system of Miocene age characterized by abundant submarine channels. This Miocene turbidite system is characterized by abundant stacked submarine channel fills such that there are only piecewise continuous horizons within the zone of interest. Such complexity is more amenable to 3D volumetric interpretation using 3D visualization, geobodies, and, in this paper, volumetric facies mapping. Animation through time slices provides a quick look at the geomorphology (Figure 2), but because of subsidence, no single time slice displays the complete depositional system. In this study, we interpreted a continuous reflector below our zone of interest and then used this horizon to generate a phantom horizon (horizon A) within the Miocene turbidite system. We then assume that deposition along horizon A represents a consistent geologic time interval. Figure 3 shows the seismic amplitude along horizon A, in which we identify stacked channels (white arrows), high-amplitude deposits (blue arrow), and slope fans (red arrow), which are also shown in Figure 2. On this phantom horizon slice, another weaker, sinuous channel (black arrow) can be identified, which cannot be seen on the time slice in Figure 2.

Attribute expression

Rather than replacing human interpreters, a good facies analysis workflow builds on the interpreter's experience and objectives. Given sufficient time, interpreters should be able to identify all the facies in a high-quality data volume. With less time, important but subtle facies and spatial relationships might be overlooked. In this work, seismic attributes quantify key features in the amplitude data for subsequent computer analysis. Amplitude and frequency attributes are often lithology indicators that may be hydrocarbon indicators in conventional reservoirs; geometric attributes quantify reflector morphology, such as dip, curvature, rotation, and convergence; statistical attributes provide information about data distribution that quantifies subtle patterns that may be easy to identify but hard to define (Chopra and Marfurt, 2007). Attributes such as coherence provide images of the edges of seismic facies rather than a measure of the facies themselves, although slumps often appear as a suite of closely spaced faults separating rotated fault blocks. Because our objective is to map a deepwater channel system consisting of incised and multistoried channels, levees, point bars, channel flanks, slope fans, and slumps, we generate attributes that highlight these features. Peak spectral frequency and magnitude can be used to differentiate thick from thin channels and overbank deposits. Reflector convergence differentiates conformal reflectors from pinch-outs and angular unconformities. Gray-level cooccurrence matrix (GLCM) attributes are texture attributes

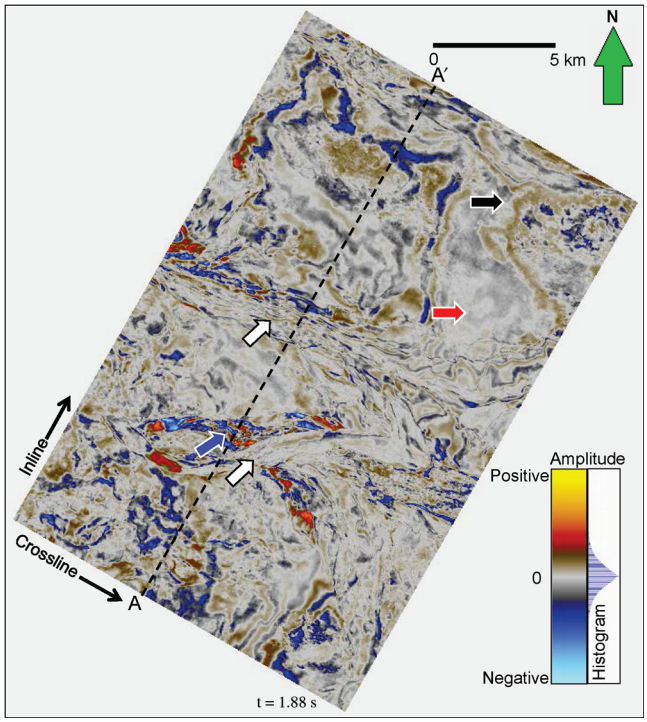

Figure 2. Time slice at $t = 1.88$ s through the seismic amplitude volume. The white arrows indicate potential channel/canyon features. The blue arrow indicates a high-amplitude feature. The red arrow indicates a relatively low energy, gently dipping area. The black arrow is explained in Figure 3. AA′ denotes a vertical cross section shown in Figure 7.

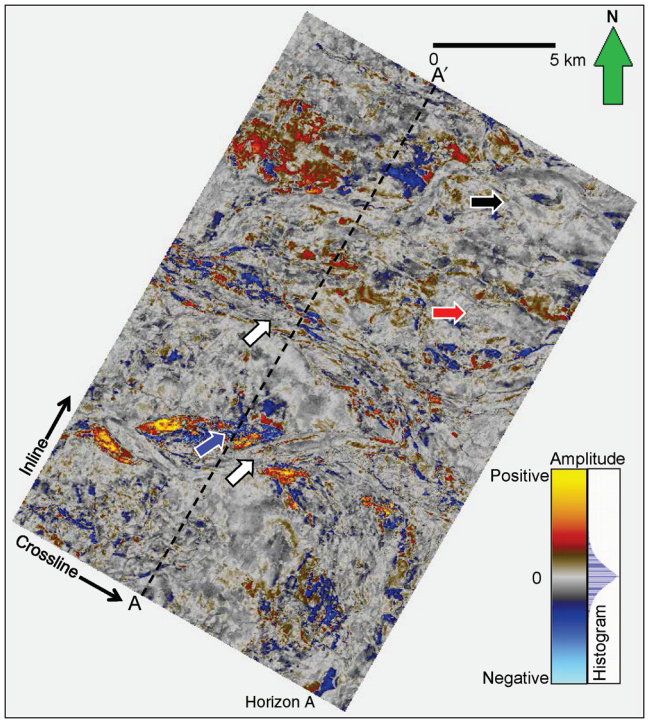

Figure 3. Horizon slice along horizon A through the seismic amplitude volume. The white arrows indicate potential channel/canyon features. The blue arrow indicates a high-amplitude feature. The red arrow indicates a relatively low energy, gently dipping area. The black arrow indicates a sinuous channel complex that is not seen in the time slice shown in Figure 2. AA′ denotes a cross section shown in Figure 7.

representing the degree of disorder, quantifying subtle variation in the depositional environment, and they are useful to characterize geomorphology changes within channel beds, channel flanks, and slope fans. Similarity (coherence) attributes help to detect edges compartmentalizing different deposition features.

Proper display of generated attributes is almost as important as selecting the suitable attributes, and corendering certain attributes correctly will greatly enhance the interpretability of an image. Using an HLS color model, we follow Marfurt (2015) to display the generated attributes in the subsequent combinations, and the rule of thumb is to display one background attribute against hue, one modulating attribute against saturation, and one calibration attribute against lightness. Figure 4 shows phantom horizon A through the peak spectral frequency corendered with peak spectral magnitude that emphasizes the relative thickness and reflectivity of the turbidite system and the surrounding slope fan. The edges of the channels are delineated by Sobel filter similarity. We show the same phantom horizon A through (Figure 5) the corendered shape index and curvedness and through (Figure 6) GLCM homogeneity corendered with coherent energy. In Figure 7, we show vertical slices at line AA′ in Figure 3 through seismic amplitude (Figure 7a), seismic amplitude corendered with peak spectral magnitude/peak spectral frequency (Figure 7b), seismic amplitude corendered with shape index and curvedness (Figure 7c), and seismic amplitude corendered with GLCM homogeneity and coherent energy (Figure 7d). The block arrows indicate several of the key facies, the white being channels, the blue being high amplitude deposits, and the red being a slope fan.

From the generated attributes, we note that two main channels (white arrows in Figures 4–7) exhibit medium-low frequency, low peak spectral magnitude, a valley shape, and low coherent energy, suggesting mud fill. Depending on which part of the channel we examine GLCM homogeneity ranges from low to medium, indicating significant complexity within the meander valley because of the frequent change in the channel route. Also note several sinuous channel complexes developed at this level (black arrows in Figures 4–6), with attribute responses generally similar to those of the two main channels. Some high-amplitude reflectors are indicated by the blue arrows in Figures 4–6, which suggest sand deposits, but it is unclear whether they are point bar or levee deposits. In most of the survey area,

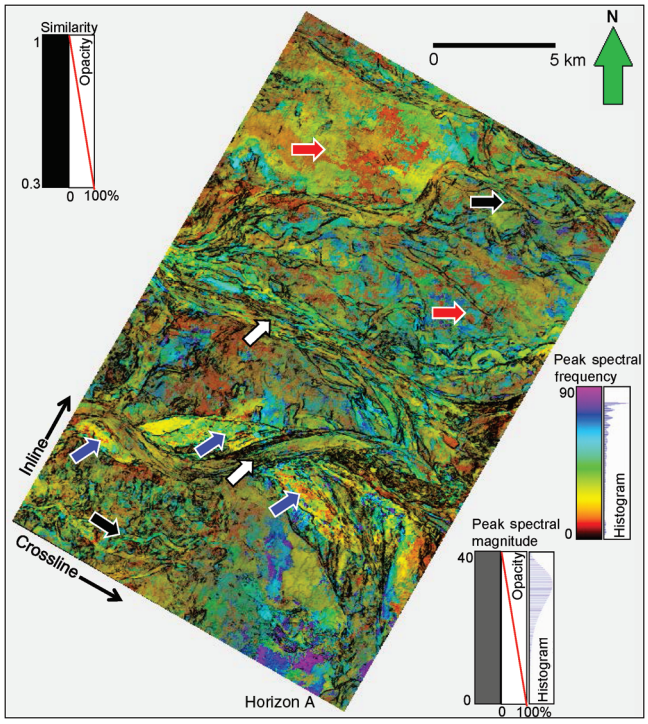

Figure 4. Horizon slice along horizon A through the peak spectral frequency corendered with peak spectral magnitude volumes. These spectral attributes computed using a continuous wavelet transform emphasize the relative thickness and reflectivity of the turbidite system and surrounding slope fan sediments into which it was incised. The edges of the channels are delineated by Sobel filter similarity. The white arrows indicate two straight to meandering main channels; the black arrows indicate sinuous channel complexes; the blue arrows indicate high-amplitude reflectors; and the red arrows indicate gently dipping slope fans.

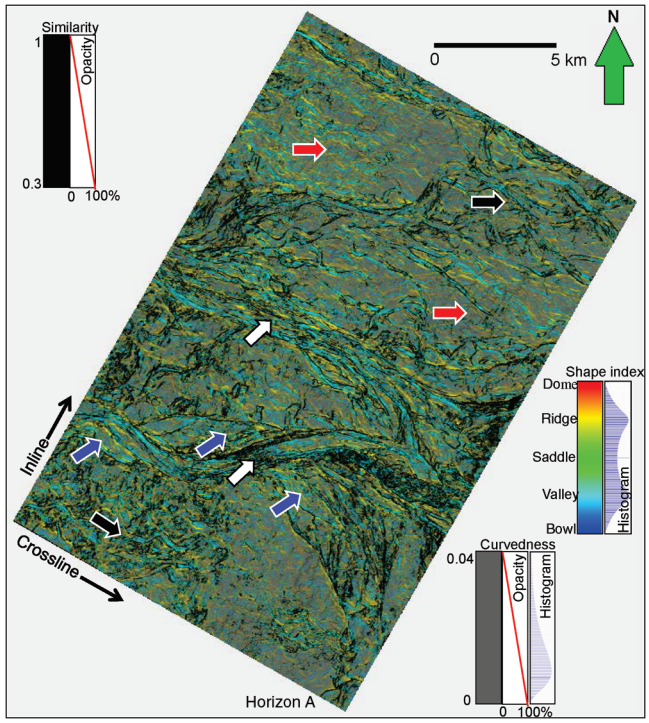

Figure 5. Horizon slice along horizon A through the corendered shape index, curvedness, and Sobel filter similarity volumes. The shape index corendered with curvedness is good for visual classification but dominates the unsupervised classifications with valley and ridge features across the survey. The white arrows indicate two straight to meandering main channels; the black arrows indicate sinuous channel complexes; the blue arrows indicate high-amplitude reflectors; and the red arrows indicate gently dipping slope fans.

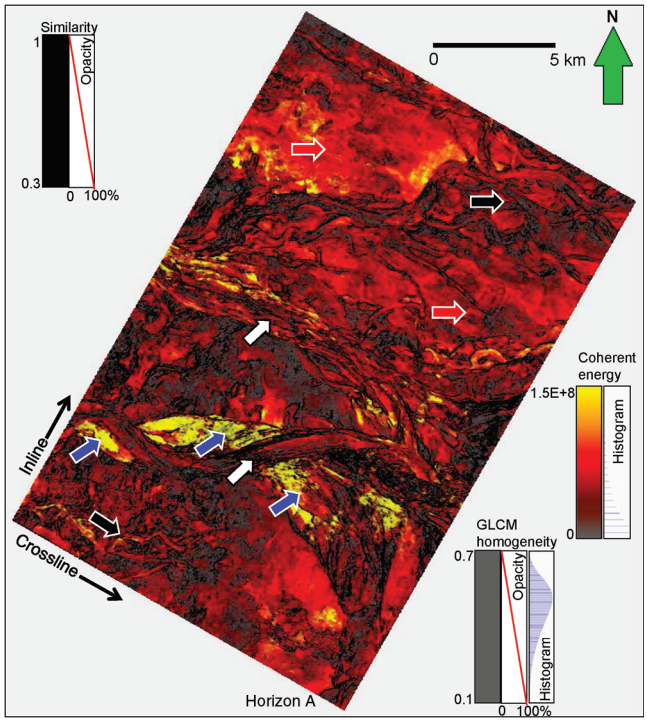

Figure 6. Horizon slice along horizon A through the corendered GLCM homogeneity, coherent energy, and Sobel filter similarity volumes. Bright colors highlight coherent, high-energy areas that indicate potential sand deposits. The white arrows indicate two straight to meandering main channels; the black arrows indicate sinuous channel complexes; the blue arrows indicate high-amplitude reflectors; and the red arrows indicate gently dipping slope fans.

there are highly homogeneous, medium energy, relatively flat reflectors, which are probably slope fans (the red arrows in Figures 4–7).

Using corendering, we are able to display and analyze two or three attributes simultaneously. However, we cannot use visualization to meaningfully combine the information content of all the attributes into a single image. Seismic facies classification techniques use multiple attributes as input to generate a facies map. Barnes and Laughlin (2002) conclude that the appropriate choice of attributes is the most critical component of computer-assisted seismic facies identification. The number of attributes should be as small as possible to discriminate the facies of interest. Each attribute should be mathematically independent of the others. In contrast, attributes should be correlated through the underlying geology, forming a pattern or waveform in the attribute space. We also need to be aware that because human eyes and computers see the same image differently (a human sees features as combinations of different textures, whereas a computer only see "voxels"), attributes that are suitable for visual interpretation may not be appropriate for use in classification. In our study, we find that the shape index dominates the unsupervised classifications with valley and ridge features across the survey, which "contaminate" the facies map. In this particular case, GLCM homogeneity anomalies follow a similar trend as the low coherent energy, such that we decide not to use GLCM homogeneity as an input attribute to reduce the redundancy. Our final group of input attributes for classification consists of peak spectral frequency, peak spectral magnitude, coherent energy, and curvedness. Figure 8

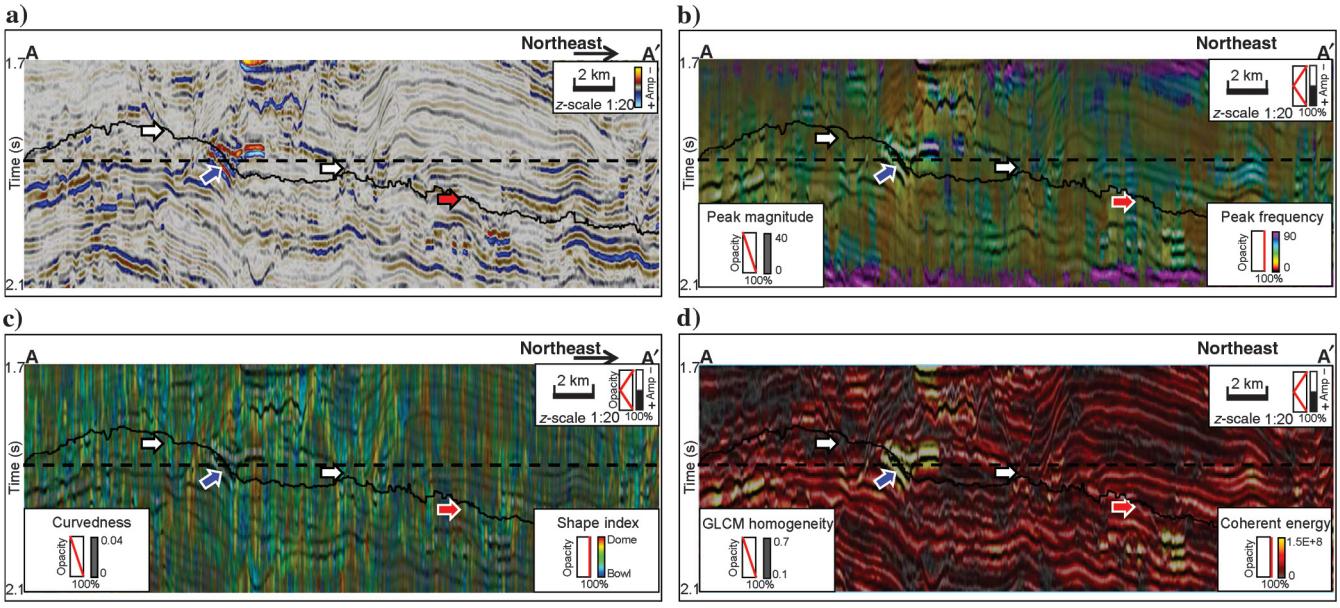

Figure 7. Vertical sections along line AA′ (location shown in Figures 2 and 3) through (a) seismic amplitude, (b) seismic amplitude corendered with peak spectral magnitude and peak spectral frequency, (c) seismic amplitude corendered with shape index and curvedness, and (d) seismic amplitude corendered with GLCM homogeneity and coherent energy. The white arrows indicate channel and canyon features. The blue arrows indicate a high-amplitude reflector. The red arrows indicate relatively low amplitude, gently dipping areas. The solid black line indicates horizon A, and the dashed black line indicates time slice $t = 1.88$ s.

shows crossplots for every attribute pair on which we see very limited correlation. Such independence is the key to successful seismic classification techniques.

SOM AND DPSOM

Seismic attributes serve as input to modern seismic classification techniques. Most geophysicists are familiar with SOM as a waveform classification technique, in which the input "attributes" are amplitudes along adjacent phantom horizon slices (Poupon et al., 1999). Coléou et al. (2003) and Strecker and Uden (2002) show how a suite of attributes can form a vector at each voxel. With this insight, we see that waveform classification and multiattribute analysis are one and the same. The waveforms or attribute vectors are represented by a finite number of prototype vectors, each of which is assigned a unique color.

In traditional Kohonen SOM, the position of an SOM node in the SOM latent space is only based on the distance between the corresponding prototype vector (the projection of an SOM node in the input data space) and the nearest data vector in the input space. DPSOM adds a step of adjusting the position of all SOM nodes accord-

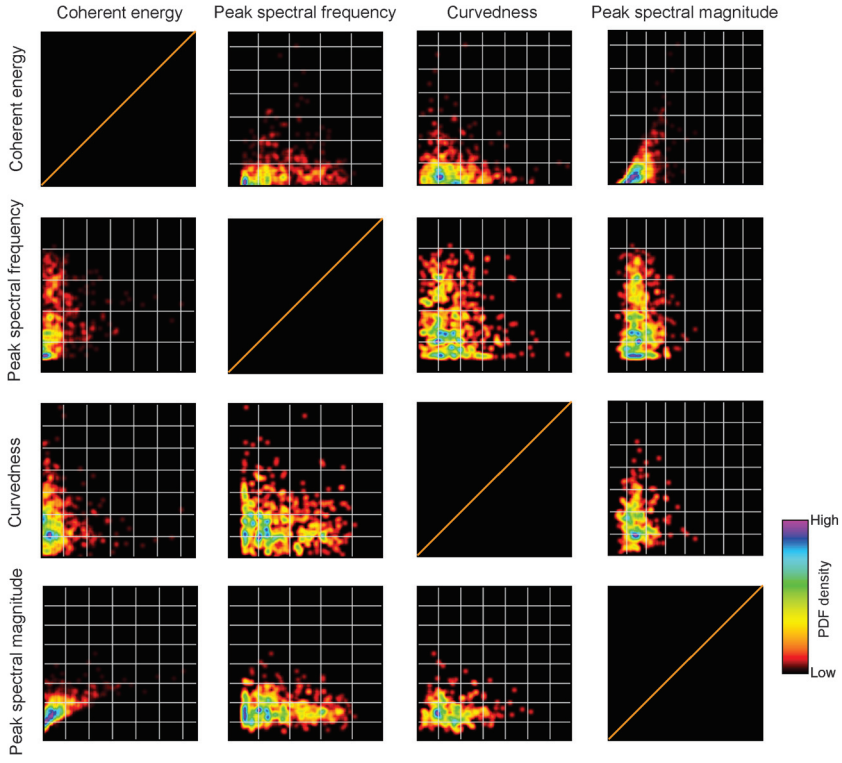

Figure 8. Crossplot among all input attribute pairs. Note that all crossplots are in a cloud shape instead of following a straight diagonal line. Such behavior demonstrates that these four attributes are relatively independent.

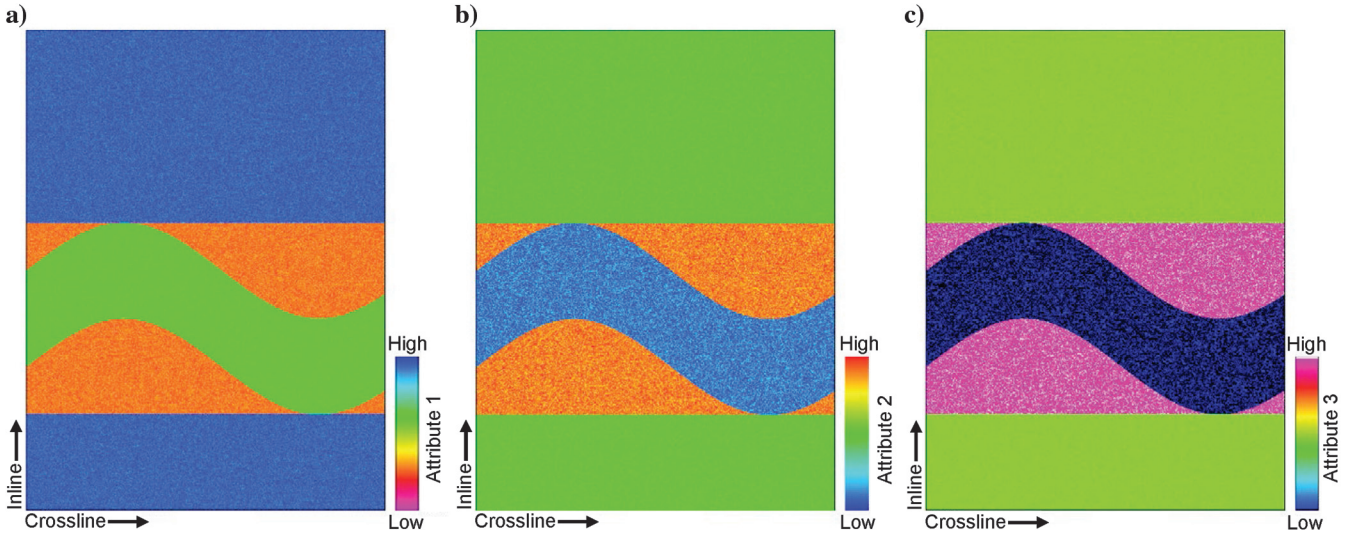

Figure 9. (a-c) Time slices through three synthetic seismic attribute volumes, delineating three seismic facies.

ing to their distances from the current winning node (best matching unit) in the input data space and SOM latent space. The adjustment rule is given by the following equation (Shao and Yang, 2012):

$$\mathbf{p}_k(t+1) = \mathbf{p}_k(t) + \alpha(t) \cdot \left(1 - \frac{\delta_{vk}}{d_{vk}}\right) \cdot (\mathbf{p}_v(t) - \mathbf{p}_k(t)), \quad \forall\, k \neq v, \tag{1}$$

where $\mathbf{p}_k(t)$ is the position of an SOM node before adjustment; $\mathbf{p}_k(t+1)$ is the position of an SOM node after adjustment; $\mathbf{p}_v(t)$ is the position of the current winning node; δ_{vk} and d_{vk} are the distance between an SOM node and the current winning node in input data space and SOM latent space, respectively. Here, $\alpha(t)$ is the learning rate that exponentially decays over iterations.

In our implementation, the SOM latent space is a 2D space initialized using the first two principal components from PCA. Defined by equation 1, an SOM node may either move toward or away from the current winning node in the SOM latent space to preserve their distance found in the input data space.

We generate a synthetic consisting of three attributes to test the proposed DPSOM algorithm and compare it with traditional SOM (Figure 9). All attribute values are randomly generated within a certain range for each facies. Table 1 summarizes the ranges for each facies on each attribute. Our model consists of three facies: a mud-filled channel, a gas-charged levee, and a flood plain.

We feed these three synthetic attributes into traditional Kohonen SOM and DPSOM with (over defined) 256 prototype vectors, and the results are shown in Figure 10. Note the traditional SOM generates a facies map with two facies (Figure 10a), splitting the flood plain into levee and channel facies. In contrast, DPSOM generates three facies, even though there are some local variations in the flood plain and levee facies (Figure 10b). The corresponding SOM latent spaces are shown in Figure 10c and 10d, in which the color for each cluster represents the histogram count. We clearly see two clusters as end members in the traditional SOM, in which we have three clusters in the DPSOM, two of which are further subdivided into two adjacent subclusters. Moreover, in Figure 10d, we clearly see that the distance between the green cluster (channel) and the cadet blue cluster (flood plain) is less than the distance between the cadet blue cluster and the deep pink cluster (levee). This is consistent with the model setting in which the attribute value ranges of the flood plain are closer to that of a channel than to that of a levee. Such a result confirms the advantage of the distance-preserving character in DPSOM over traditional SOM.

Application

Given the selected four attributes, we form 4D attribute vectors at each voxel and feed them into the DPSOM classification algorithm. As interpreters, we need to validate the final classifications to determine if they delineate the seismic facies of interest. In our example, we use a Sobel filter similarity to separate

Table 1. Value ranges for each facies on each attribute. All values are randomly generated within the given range.

Facies	Attribute		
	Attribute 1	Attribute 2	Attribute 3
Shale-filled channel	25–30	−0.7 to −0.4	0–2
Gas-charged levee	10–15	0.4–0.7	10–15
Flood plain	40–45	−0.1–0.1	4–6

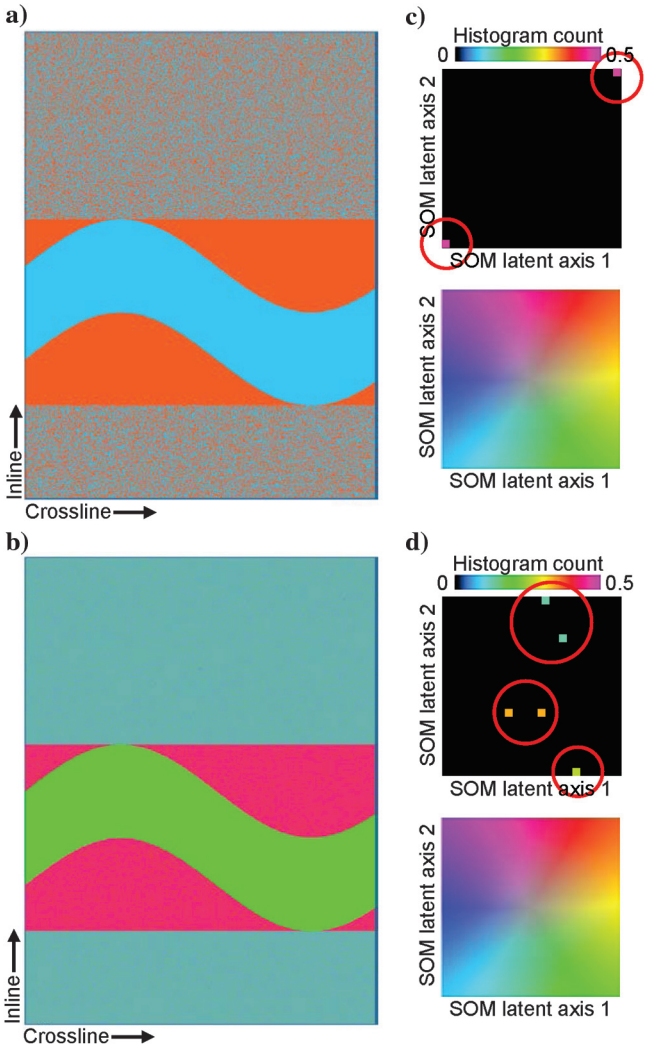

Figure 10. Classification result using (a) traditional SOM and (b) DPSOM for the synthetic data shown in Figure 9. (c) Corresponding SOM latent spaces and 3D colorbars for panels (a) and (d). Clusters in the upper figures in panels (c and d) are colored according to their corresponding position in the 2D colorbar. For example, a cluster appears in the upper left corner of the SOM latent space is colored in orange (the color in the upper left corner of the 2D colorbar) in the seismic faces map.

the facies and then evaluate how they fit within our understanding of a turbidite system.

To ensure the DPSOM classifier is analyzing data in a relatively constant depositional environment, we take a 100 ms analysis window centered about phantom horizon A. In this window, each voxel (inline, crossline, and time) is represented by a 4D data vector (peak spectral frequency, peak spectral magnitude, coherent energy, and curvedness). After normalizing the input data along each dimension using the Mahalanobis distance (Mahalanobis, 1936), a 2D SOM latent space is initialized using the first two principal components. We then take one of every 125 data vectors (every fifth inline, crossline, and time sample) as training data to construct the SOM model. For each SOM training iteration, the position of all SOM nodes is adjusted based on equation 1, resulting in a SOM model that honors the distance among data vectors in the 4D input space. Once the algorithm reaches the desired number of iterations (in our case, five iterations), the SOM model is applied to the data within the analysis window. Using only a single processor, the total calculation time is approximately 10 min, for a 25 sample by 600 inline by 1800 crossline data slab of four attribute data.

Figure 11 shows the DPSOM classification result along phantom horizon A. In the upper right corner, we show a 2D colorbar and a 2D histogram representing the classes in the SOM latent space, with the two axes being the first two principal components of the 4D input data. We then color code the classes using the 2D colorbar, and we paint each sample point in the 3D seismic volume using the same color as the class to which it belongs. To better illustrate the distance-preserving characteristic of DPSOM, we compare with the result from the classic Kohonen SOM using the same parameters (Figure 12). It is observed that different geologic features in Figure 11 are represented by more distinct colors than in Figure 12. For example, the sinuous channel complex in the far north is more visually segmented from the surrounding slope fan in Figure 11 than in Fig-

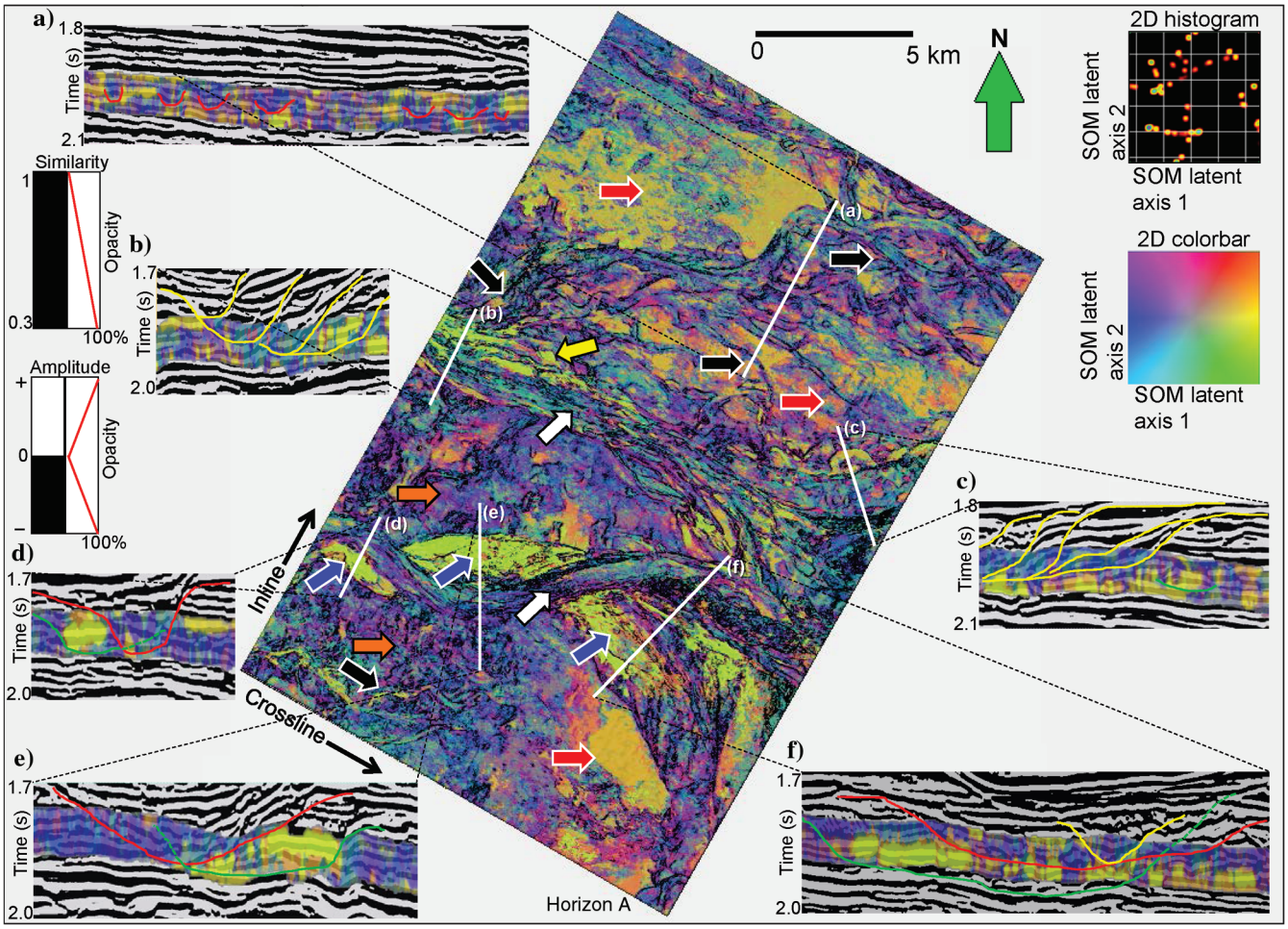

Figure 11. Slice along horizon A through the seismic facies map generated from DPSOM using a 2D colorbar. The white arrows indicate two straight to meandering mud-filled channels. The blue arrows indicate a possible sand-filled channel that is cut through by one of the mud-filled channels. The red arrows indicate possible slope fan and lobe deposits. The black arrows indicate sinuous channel complexes. The yellow arrow indicates possible sand-filled lateral accretion packages. Sections (a-f) are vertical sections of corendered seismic amplitude and SOM facies demonstrating the morphology of the channel complexes in vertical profiles. The displayed SOM facies volume is centered at horizon A.

ure 12. This is attributed to the distance between these two facies being better preserved in DPSOM; therefore, the contrast between colors representing such facies is greater in Figure 11. Back to Figure 11, we then identify two main slope channels (white arrows) that are classified as cyan that converge downstream. Vertical slices show these both to be multistory channels. As the channels move downslope, the slope becomes gentler, such that sediments lose momentum, spread out, and form a lobate feature. The black arrows indicate several sinuous channel complexes. On the facies map, we see the northernmost large channel complex bifurcating into two minor channels. Most of the channel fill appears as cyan, similar to the two main channels, which suggests they are probably mud filled. The coherent slope fans (indicated by red arrows) are characterized by brownish colors. The purplish color facies (orange arrows) are less coherent and may indicate massive turbidite current or slump deposits. The yellow arrow indicates an older, probably sand-filled channel within the multistoried system. The blue arrows indicate the same color facies that we interpreted to be an older, high-energy, sand-filled channel developed earlier than the mud-filled channel cutting through it. This sand-filled channel spreads out and contributes to the lobe further downslope where it is covered by mud deposits transported by later stage channels.

In Figure 11a–11f, we also show several vertical slices through a corendered seismic amplitude with SOM facies volumes. In each image, phantom horizon A is vertically centered within the SOM analysis window. Figure 11a shows the smaller scaled channels in the northern channel complex. We use red lines to delineate the longitudinal profile of the channels. We find the channels are mapped in cyan to purple colors, with the surrounding overbank complex deposits mapped in yellow to brown colors. This contrast in color has greatly simplified the characterization of such channel complexes, which otherwise are extremely tedious to interpret on traditional seismic amplitude data. Figure 11b displays the lateral migration of the northern main channel complex. In this vertical section, we identify at least four channel stories migrating from northeast to southwest (the yellow lines highlight different stories). We notice that the oldest story is mapped as lime green, whereas the younger channels are cyan (with the youngest one out of the SOM analysis window). This suggests a change of lithology during deposition, with the oldest story sand filled, and the younger stories mud filled. Figure 11c shows the vertical profile of the more distal northern main channel. Comparing to section Figure 11b, which is more proximal, the distal part of the channel is more spread out, forming a lobe mixed with the southern main channel. We also see an oxbow-like feature (probably another sandy channel fill) in the older deposits (outlined in green). Figure 11d–11f shows three vertical profiles through the proximal to distal portions of the southern main channel (outlined in red), in which we clearly see it cutting through an older sand-filled channel in lime green (outlined in green). Similar to the northern main channel, we see that the width of the southern channel (and the old sand-filled channel) has expanded dramatically from proximal to distal, merging with the northern lobe. The yellow line in Figure 11f highlights a younger mud-filled incised channel in the southern main channel.

In Figure 13, we show four prototype vectors representing four key facies. The location of the prototype

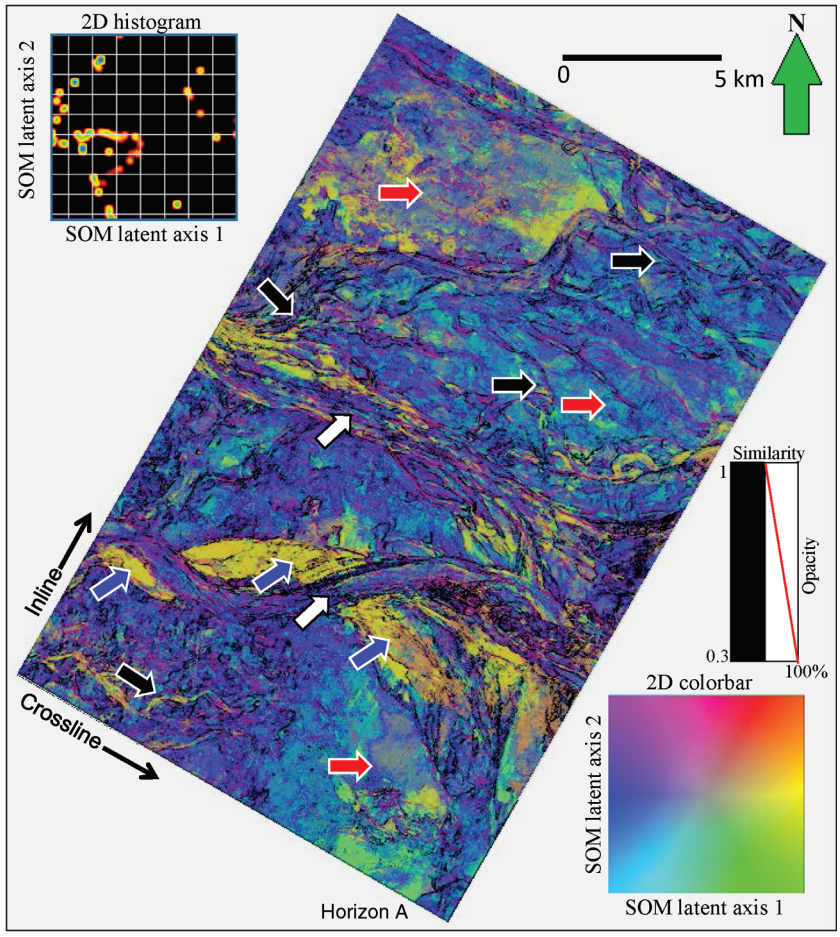

Figure 12. Slice along horizon A through the seismic facies map generated from classic Kohonen SOM using a 2D colorbar. The white arrows indicate two straight to meandering mud-filled channels. The blue arrows indicate a possible sand-filled channel that is cut through by one of the mud-filled channels. The red arrows indicate possible slope fan and lobe deposits. The black arrows indicate sinuous channel complexes. Note the less separated facies represented by more similar colors compared to Figure 11.

vector in the 3D inline-crossline-time space and 2D SOM latent space is shown in Figure 13a, whereas the normalized attribute responses of these four prototype vectors are shown in Figure 13b. To ensure that the prototype vectors correctly represent the facies they belong to, all the attribute responses in Figure 13b are averaged from a five-sample × five-trace × five-trace window centered at the target prototype vectors. As expected, the prototype vectors in similar facies (colors) have similar attribute responses. Prototype vector 1 is selected to represent sand-filled channel deposits, which has a similar response to that of prototype vector 3, which is selected to represent sandy overbank complexes. The interchannel overbank complex (prototype vector 2) and the mud-filled sinuous channel complex (prototype vector 4) are in similar facies (blue to purple colors) and have different attribute responses. We also show the difference in reflection characteristics of the multistoried channel (yellow circle) and older sand-filled channel (blue circle) that are in similar SOM facies. All such interpretations are solely based on seismic amplitude data, which need to be further verified by well log or core analysis.

Conclusions

In this study, we are able to characterize a Miocene deepwater turbidite system in Canterbury Basin, New Zealand, by incorporating seismic attributes, seismic facies classification, and a limited amount of structural interpretation (picking one horizon). Phantom horizon slices through seismic attribute volumes effectively delineate depositional features in which there are no continuous surfaces to pick. Corendering seismic attributes against an HLS color model facilitates the visual integration of two or three attributes at the same time, which greatly increases the value of seismic attributes. DPSOM is an innovative classification technique that produces an improved classification result by preserving the distance in input data space. The seismic facies map generated from DPSOM using appropriate seismic attributes provides statistics-based machine assistance to identify depositional facies in a turbidite system. Multiple sinuous channel complexes and multistory channel stacking patterns are delineated precisely along with their depositional patterns, which can be further used to locate potential reservoirs.

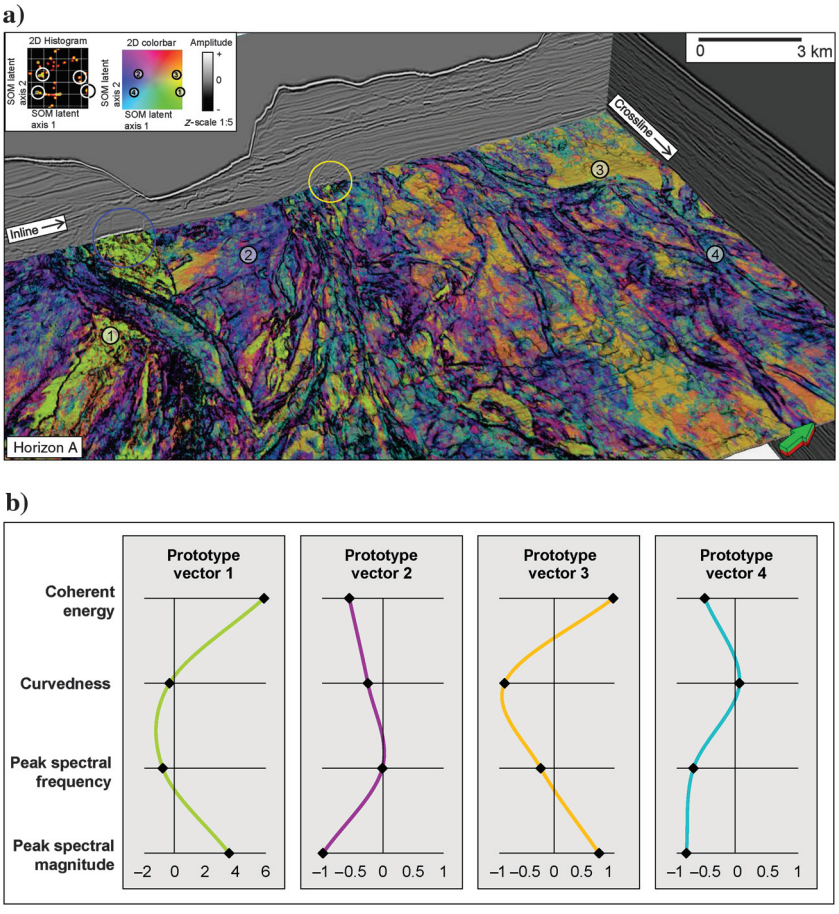

Figure 13. (a) Three-dimensional chair display of the SOM facies map along horizon A with orthogonal vertical slices through seismic amplitude. The location of four prototype vectors is shown on the facies map and on the 2D histogram and colorbar. Also note the similarity in classification of what we interpret to be an older sand-filled channel (blue circle) and a discrete sand-filled channel that forms part of a multistoried channel complex (yellow circle). (b) Seismic attribute responses of the four prototype vectors. Input attributes are coherent energy, curvedness, peak spectral frequency, and peak spectral magnitude. All attribute values are normalized using a z-scale.

Acknowledgments

We thank New Zealand Petroleum and Minerals for providing the Waka-3D seismic data to the public for use in research and education. Financial support for this effort is provided by the sponsors of the Attribute-Assisted Seismic Processing and Interpretation (AASPI) Consortium at the University of Oklahoma. We thank our colleagues for their valuable input and suggestions. All the 3D seismic displays were made using licenses to Petrel provided to the University of Oklahoma for research and education courtesy of Schlumberger.

References

Barnes, A. E., 2007, Redundant and useless seismic attributes: Geophysics, **72**, no. 3, P33–P38, doi: 10.1190/1.2716717.

Barnes, A. E., and K. J. Laughlin, 2002, Investigation of methods for unsupervised classification of seismic data: 72nd Annual International Meeting, SEG, Expanded Abstracts, 2221–2224.

Chopra, S., and K. J. Marfurt, 2007, Seismic attributes for prospect identification and reservoir characterization: SEG.

Coléou, T., M. Poupon, and K. Azbel, 2003, Unsupervised seismic facies classification: A review and comparison of techniques and implementation: The Leading Edge, **22**, 942–953, doi: 10.1190/1.1623635.
Himberg, J., 2000, A SOM based cluster visualization and its application for false coloring: Proceedings of the IEEE-INNS-ENNS International Joint Conference on Neural Networks, IEEE **3**, 587–592.
Kohonen, T., 1982, Self-organized formation of topologically correct feature maps: Biological Cybernetics, **43**, 59–69, doi: 10.1007/BF00337288.
Mahalanobis, P. C., 1936, On the generalized distance in statistics: Proceedings of the National Institute of Sciences of India, **2**, 49–55.
Marfurt, K. J., 2015, Techniques and best practices in multiattribute display: Interpretation, **3**, B1–B23, doi: 10.1190/INT-2014-0133.1.
Merkl, D., and A. Rauber, 1997, Alternative ways for cluster visualization in self-organizing maps: Proceedings of the Workshop on Self-Organizing Maps (WSOM97), Helsinki University of Technology, 106–111.
Mitchell, J., and H. L. Neil, 2012, OS20/20 Canterbury — Great South Basin TAN1209 voyage report: National Institute of Water and Atmospheric Research Ltd. (NIWA).
Poupon, M., K. Azbel, and G. Palmer, 1999, A new methodology based on seismic facies analysis and litho-seismic modeling: The Elkhorn Slough field pilot project, Solano County, California: 69th Annual International Meeting, SEG, Expanded Abstracts, 927–930.
Roy, A., B. L. Dowdell, and K. J. Marfurt, 2013, Characterizing a Mississippian tripolitic chert reservoir using 3D unsupervised and supervised multiattribute seismic facies analysis: An example from Osage County, Oklahoma: Interpretation, **1**, SB109–SB124, doi: 10.1190/INT-2013-0023.1.
Rubio, M., and V. Gimnez, 2003, New methods for self-organising map visual analysis: Neural Computing and Applications, **12**, 142–152, doi: 10.1007/s00521-003-0387-7.
Shao, C., and Y. Yang, 2012, Distance-preserving SOM: A new data visualization algorithm: Journal of Software, **7**, 196–203, doi: 10.4304/jsw.7.1.196-203.
Strecker, U., and R. Uden, 2002, Data mining of 3D post-stack attribute volumes using Kohonen self-organizing maps: The Leading Edge, **21**, 1032–1037, doi: 10.1190/1.1518442.
Sutherland, R., and G. Browne, 2003, Canterbury basin offers potential on South Island, New Zealand: Oil & Gas Journal, **101**, 45–49.
Uruski, C. I., 2010, New Zealand's deepwater frontier: Marine and Petroleum Geology, **27**, 2005–2026, doi: 10.1016/j.marpetgeo.2010.05.010.
Wang, D., H. Ressom, M. Musavi, and C. Domnisoru, 2002, Double self-organizing maps to cluster gene expression data: Proceedings of 2002 European Symposium on Artificial Neural Networks, d-side publishing, 45–50.
Zhang, B., T. Zhao, X. Jin, and K. J. Marfurt, 2015, Brittleness evaluation of resource plays by integrating petrophysical and seismic data analysis: Interpretation, **3**, T81–T92, doi: 10.1190/INT-2014-0144.1.
Zhao, T., V. Jayaram, A. Roy, and K. J. Marfurt, 2015, A comparison of classification techniques for seismic facies recognition: Interpretation, **3**, SAE29–SAE58, doi: 10.1190/INT-2015-0044.1.

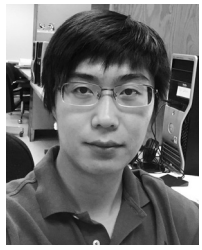

Tao Zhao received a B.S. (2011) in exploration geophysics from the China University of Petroleum and an M.S. (2013) in geophysics from the University of Tulsa. He is currently pursuing a Ph.D. in geophysics at the University of Oklahoma as a member of the AASPI Consortium. His current research interests include developing and applying pattern recognition and machine learning techniques on seismic data, unconventional shale resource play characterization, and seismic attribute development.

Jing Zhang received a B.S. in geology and geophysics from the Missouri University of Science and Technology and an M.S. (2014) from the University of Oklahoma. Her current research interests include comprehensive unconventional reservoir characterization of the Woodford Shale in Oklahoma. She is skilled in sequence stratigraphy, sedimentology, seismic interpretation, and well log interpretation.

Fangyu Li received B.S. (2009) and M.S. (2013) degrees in electrical engineering from Beihang University and Tsinghua University, respectively. He is pursuing a Ph.D. in geophysics at the University of Oklahoma. His research interests include seismic processing, quantitative seismic interpretation, and seismic attribute development.

Kurt J. Marfurt received a Ph.D. (1978) in applied geophysics from Columbia University's Henry Krumb School of Mines in New York. He joined The University of Oklahoma in 2007, where he teaches geophysics. His career includes 18 years with Amoco Research and 20 years in academia. He teaches short courses on attributes for SEG and AAPG and currently serves as editor of *Interpretation*. His primary research interest includes the development and calibration of new seismic attributes to aid in seismic processing, seismic interpretation, and reservoir characterization, with a focus on resource plays.